

A Dynamic Kernel Prior Model for Unsupervised Blind Image Super-Resolution

Zhixiong Yang¹ Jingyuan Xia^{1,*} Shengxi Li² Xinghua Huang¹
 Shuanghui Zhang¹ Zhen Liu¹ Yaowen Fu¹ Yongxiang Liu¹

¹College of Electronic Engineering, National University of Defense Technology, Changsha, China

²College of Electronic Engineering, Beihang University, Beijing, China

yzx21@nudt.edu.cn, j.xia10@nudt.edu.cn

Abstract

Deep learning-based methods have achieved significant successes on solving the blind super-resolution (BSR) problem. However, most of them request supervised pre-training on labelled datasets. This paper proposes an unsupervised kernel estimation model, named dynamic kernel prior (DKP), to realize an unsupervised and pre-training-free learning-based algorithm for solving the BSR problem. DKP can adaptively learn dynamic kernel priors to realize real-time kernel estimation, and thereby enables superior HR image restoration performances. This is achieved by a Markov chain Monte Carlo sampling process on random kernel distributions. The learned kernel prior is then assigned to optimize a blur kernel estimation network, which entails a network-based Langevin dynamic optimization strategy. These two techniques ensure the accuracy of the kernel estimation. DKP can be easily used to replace the kernel estimation models in the existing methods, such as Double-DIP and FKP-DIP, or be added to the off-the-shelf image restoration model, such as diffusion model. In this paper, we incorporate our DKP model with DIP and diffusion model, referring to DIP-DKP and Diff-DKP, for validations. Extensive simulations on Gaussian and motion kernel scenarios demonstrate that the proposed DKP model can significantly improve the kernel estimation with comparable runtime and memory usage, leading to state-of-the-art BSR results. The code is available at <https://github.com/XYLGroup/DKP>.

1. Introduction

Deep learning provides a new avenue for solving the blind super-resolution (BSR) problem, which aims to reconstruct

Zhixiong Yang and Jingyuan Xia contributed equally to this work (*Corresponding author: Jingyuan Xia). This work is supported by National Natural Science Foundation of China, projects 61921001, 62131020, 62322121 and 62171448, and the NSFDYS of Hunan 2022J110067.

high-resolution (HR) images from the low-resolution (LR) observations with unknown blur kernels, and is known to be highly non-convex and ill-posed. To alleviate the non-convexity and ill-posedness, most of learning-based BSR methods incorporate image priors via supervised learning based on paired LR-HR samples. However, pre-defined labeled training datasets are expensive, time-consuming, and even not feasible in specific scenarios, such as for high speed targets (e.g., satellites, aircraft) and medical images (e.g., beating heart). Thus, unsupervised learning-based solutions are highly demanded for BSR problem.

The existing BSR methods can be roughly divided into model-based and learning-based strategies in terms of the priors adopted to provide performance guarantee. Model-based approaches [19, 21, 33, 51] typically adopt hand-designed and explicit constraints as regularizations on image properties, or expert knowledge of the blur kernel. Meanwhile, learning-based BSR methods [12, 16, 20, 27–29, 49, 53, 54, 56] aim to train an end-to-end network with paired LR-HR image samples to leverage data priors for boosting performances. However, these methods highly demand the data and need to undergo thorough pre-training before applications, leading to limited generalization ability towards varying blur kernels. To alleviate this issue, quite a few methods [5, 13, 40, 50, 57, 59] substitute the cumbersome training in advance by a well-trained diffusion model with significantly less fine-tuning samples in an off-the-shelf fashion. On the other side, a slice of works [3, 17, 25, 34, 39, 51] propose to replace the HR image data priors by kernel priors, which are more substantial, economical and efficient to be trained. However, both of these advances are underlying the supervised learning scheme with necessity of training on labeled datasets, still hindering the flexibility and generalization ability towards the BSR tasks with different kernels and unknown HR ground truths.

In this paper, we propose a dynamic kernel prior (DKP) generation model that can be plug-in with the majority of image restoration (IR) models, to solve BSR problem in an

unsupervised way. The proposed DKP model consists of two modules: random kernel sampling (RKS) module and prior kernel estimation (PKE) module. In the RKS module, a Markov Chain Monte Carlo (MCMC) sampling strategy on kernel distributions iteratively generates random kernels as kernel priors, which are then assigned to the PKE module. The PKE module is employed to estimate the blur kernel with respect to the kernel prior generated from the RKS module, the observed LR input and estimated HR image from the IR model. The estimated blur kernel is then assigned to an adopted IR model for the HR image restoration. Along with the alternative solving processes, the MCMC process in RKS module converges to a desired kernel distribution with respect to the LR observation and the estimated HR image to guarantee a rational kernel prior. Meanwhile, a network-based Langevin dynamics (NLD) paradigm is proposed to optimize the kernel estimator in our PKE module with respect to the RKS output kernel prior and the data consistency based on the LR image reconstruction error. The RKS module realizes an unsupervised kernel prior learning. The PKE module achieves promising kernel estimation via the NLD update scheme, which further alleviates the non-convexity and ill-posedness in the view of optimization strategy. In this way, the DKP model is capable of providing the plug-and-play kernel estimation without training in advance on paired LR-HR samples, and is flexible to be applied to the existing IR models for solving the BSR problem.

Two applications are proposed to validate the feasibility and performance of our DKP model: deep image prior (DIP) [44] and diffusion model [14] adopted as the IR model, referring to DIP-DKP and Diff-DKP, respectively. For the DIP-DKP, we simultaneously optimize the parameters of DIP and DKP models from scratch during the alternative solution process. For the Diff-DKP, the adopted diffusion model is off-the-shelf from [14] and is applied as the fixed HR image restorer. The DKP model is optimized from scratch as well. Extensive simulation results show that the DIP-DKP achieves comparable performance than the existing methods, while the Diff-DKP achieves the state-of-the-art performance in both of Gaussian and motion kernel scenarios. The main contributions are summarized as follows:

- The RKS module is proposed to generate a rational kernel prior from the MCMC sampling on random kernel distributions. This way, an unsupervised kernel prior learning is achieved to substitute the pre-training phase.
- In PKE module, the NLD is proposed to optimize the kernel estimator, ensuring good convergence and concise estimation of the blur kernel from the perspective of optimization strategy.
- The proposed DKP model enjoys the ease use on the popular IR models without the necessity of pre-training/re-

training towards different scenarios. The two applications, i.e., DIP-DKP and Diff-DKP, validate the state-of-the-art performance and excellent flexibility of our DKP model.

2. Related Work

To alleviate the non-convexity and ill-posedness, early model-based approaches [11, 31, 33, 37] typically construct image priors in explicit formulations, such as the total variation (TV) [36], gradient profile [42], hyper-Laplacian [21] and sparsity [19]. In contrast, learning-based methods [7, 12, 16–18, 20, 28, 29, 45, 49, 53, 56] typically train an end-to-end network on labelled image samples to incorporate data priors. Wang *et al.* [45] proposed a CNN-based deep network with degradation feature representation module to learn image degradation feature from supervised training on paired LR-HR images. Li *et al.* [24] proposed a transformer network to learn multi-scale image feature via self-attention mechanisms. To reduce the high training costs of time and data, recent advances [5, 38, 40, 46, 50, 57, 59] are proposed to solve BSR problem by an off-the-shelf diffusion model [14]. Lin *et al.* [26] proposed to partially fine-tune the parameters of diffusion model with significantly less labeled images. Wang *et al.* [46] further formulated a diffusion-based BSR algorithm that iteratively solves super-resolution tasks with the given kernel without re-training. Different from the end-to-end models that are trained on paired image samples, recent methods tend to resolve BSR problem via pre-training on kernel datasets [25] or pre-defined kernel priors [51]. An alternative framework between the kernel estimation and image restoration is typically adopted in these methods [3, 10, 12, 39, 44, 58], such as double-deep image prior (Double-DIP) [34]. On the basis of this framework, Liang *et al.* [25] established a flow-based kernel prior (FKP) network that is pre-trained on labeled kernels to enroll kernel priors while the HR image is estimated by DIP network in an online fashion. Yue *et al.* [51] proposed a hand-crafted kernel prior model to improve the robustness towards the Gaussian kernel scenario. Despite the fact that these methods approximately bring down the data requirements and training costs, the necessity of training in advances or hand-crafted design still limits the flexibility and generalization ability towards the varying kernel scenarios (Gaussian and motion) without ground truths.

3. Dynamic Kernel Prior (DKP)

Problem Formulation. The degradation model of BSR problem is commonly expressed as follows,

$$\mathbf{y} = (\mathbf{x} \otimes \mathbf{k}) \downarrow_s + \mathbf{n}, \quad (1)$$

where \mathbf{y} denotes the LR image, \mathbf{x} denotes the HR image, \otimes indicates the convolution operation, \downarrow_s denotes the down-

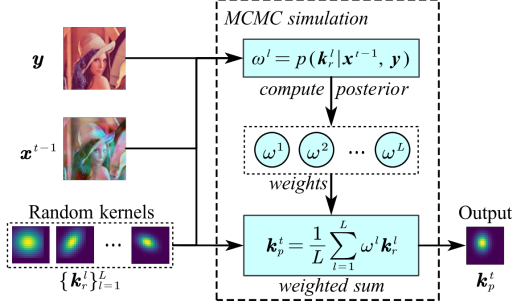


Figure 1. The overview of the RKS module. The MCMC simulation can generate the random kernel \mathbf{k}_p^t from random kernel distributions $\{\mathbf{k}_r^l\}_{l=1}^L$ as the kernel prior with respect to the current model parameters $\mathbf{x}^{t-1}, \mathbf{y}$.

sampling operation with scale factor s , and \mathbf{k} denotes the blur kernel. The BSR problem (1) can be formulated as a maximum a posteriori (MAP) problem:

$$\max_{\mathbf{x}, \mathbf{k}} p(\mathbf{y}|\mathbf{x}, \mathbf{k})p(\mathbf{x})p(\mathbf{k}), \quad (2)$$

where $p(\mathbf{y}|\mathbf{x}, \mathbf{k})$ denotes the likelihood of the observed LR image \mathbf{y} , $p(\mathbf{x})$ and $p(\mathbf{k})$ are the HR image and kernel priors, respectively. Image priors [8, 14, 41, 44, 55] have been well-designed and fully-studied in the past decade. In contrast, researches on kernel priors $p(\mathbf{k})$ are in the ascendant, as kernel samples are less expensive to obtain and the training phase is more efficient [9, 12, 25, 51, 53].

In this paper, we propose the DKP model, which comprises two modules: RKS and PKE. The RKS module is employed to generate rational kernel priors, which are assigned to the PKE module to support the estimation of blur kernel. Let $t = 1, 2, \dots, T$ denote the alternative iterations among these two modules and the adopted IR model, \mathbf{k}^t and \mathbf{x}^t denote the estimated blur kernel and HR image at the t^{th} iteration, respectively. The details of DKP model is given below.

RKS module. At the t^{th} iteration, the RKS module plays the key role of generating a rational kernel prior \mathbf{k}_p^t from the MCMC simulation. The overview diagram is shown in Fig. 1. Let $p(\mathbf{k}_r|\Sigma_r)$ denotes that the random kernel \mathbf{k}_r is conditioned by the latent variable Σ_r , in which $p(\Sigma_r)$ determines the category of blur kernel. Then the distribution of the kernel prior \mathbf{k}_p^t can be formulated as

$$p(\mathbf{k}_p^t) = \int_{\Sigma_r} p(\mathbf{k}_r|\Sigma_r)p(\Sigma_r)d\Sigma_r. \quad (3)$$

Here, Σ_r is the parameter of kernel (e.g., the variance of Gaussian kernel or the length of motion kernel). It is not easy to sample all the possible Σ_r , and therefore, we convert (3) into the Monte Carlo simulation in the following form:

$$p(\mathbf{k}_p^t) \approx \sum_{l=1}^L p(\mathbf{k}_r^l|\Sigma_r^l)\Sigma_r^l, \quad (4)$$

where l denotes the index of the Monte Carlo sampling, Σ_r^l denotes the l^{th} sampled latent variable, \mathbf{k}_r^l is the l^{th} sampled kernel, conditioned on the Σ_r^l .

To ensure the rationality of randomly generated kernels towards the BSR problem, as well as the optimization during the iterations, the MCMC simulation is proposed as follows,

$$p(\mathbf{k}_p^t|\mathbf{x}^{t-1}, \mathbf{y}) \approx \sum_{l=1}^L p(\mathbf{k}_r^l|\mathbf{x}^{t-1}, \mathbf{y})p(\mathbf{k}_r^l|\Sigma_r^l)\Sigma_r^l, \quad (5)$$

where $p(\mathbf{k}_r^l|\mathbf{x}^{t-1}, \mathbf{y})$ denotes the kernel weight ω^l , that is conditioned on the observed LR image \mathbf{y} and the estimated HR image \mathbf{x}^{t-1} with respect to the MCMC loss \mathcal{L}_{MCMC} in the following form

$$\omega^l = p(\mathbf{k}_r^l|\mathbf{x}^{t-1}, \mathbf{y}) \propto \frac{1}{\mathcal{L}_{MCMC}^l}, \quad (6)$$

where

$$\mathcal{L}_{MCMC}^l = \|\mathbf{y} - (\mathbf{x}^{t-1} \otimes \mathbf{k}_r^l) \downarrow_s\|_F^2 + \delta, \quad (7)$$

δ is the noise to prevent $\mathcal{L}_{MCMC}^l = 0$. In this way, \mathbf{k}_p^t can be formulated as

$$\mathbf{k}_p^t = \frac{1}{L} \sum_{l=1}^L \omega^l \mathbf{k}_r^l. \quad (8)$$

The obtained \mathbf{k}_p^t is then assigned to the PKE module as a rational kernel prior, which will be introduced next.

We note that the obtained kernel prior \mathbf{k}_p^t is an expectation of L times sampling according to (4). The number of the sampling times L plays the role of annealing/tempering in MCMC simulations as a hyper-parameter. Details of the tuning on L will be given in Section 5.1.

PKE module. In our DKP model, the PKE module is employed to estimate the blur kernel by a lightweight network G_k with parameters ϕ_k as follows

$$\mathbf{k}^t = G_k(\phi_k^t). \quad (9)$$

The network G_k takes a fixed noise that is randomly initialized as input, and we neglect it for demonstration convenience as ϕ_k^t are the main variables.

This kernel estimator G_k is optimized in the NLD paradigm with respect to the data-consistency term and kernel prior term, as shown in Fig. 2. The data-consistency term is computed by the LR image reconstruction error, which is given by

$$\log p(\phi_k^{t-1}|\mathbf{x}^{t-1}, \mathbf{y}) = -\|\mathbf{y} - (\mathbf{x}^{t-1} \otimes G_k(\phi_k^{t-1})) \downarrow_s\|_F^2. \quad (10)$$

The kernel prior term is computed based on the difference between the network-estimated kernel $G_k(\phi_k^{t-1})$ and the

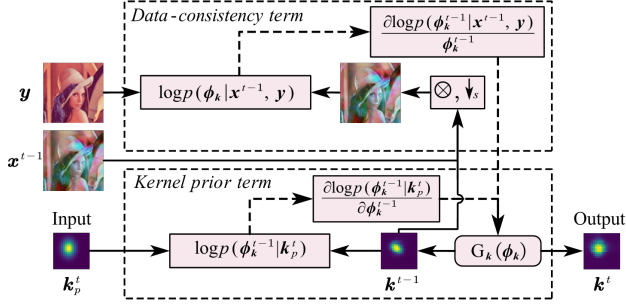


Figure 2. The overview of the PKE module. The blur kernel k^t is estimated by the network G_k , whose parameters ϕ_k are updated by the kernel prior term from RKS module and data-consistency term, based on the LR image reconstruction error.

random-sampled kernel k_p^t from the RKS module as follows,

$$\log p(\phi_k^{t-1}|k_p^t) = -\|G_k(\phi_k^{t-1}) - k_p^t\|_F^2. \quad (11)$$

By combining (10) and (11), the network parameters ϕ_k^{t-1} can be updated as follows,

$$\phi_k^t = \phi_k^{t-1} + \frac{\delta^2}{2} \frac{\partial \log p(\phi_k^{t-1}|\mathbf{x}^{t-1}, \mathbf{y})}{\partial \phi_k^{t-1}} + \delta \frac{\partial \log p(\phi_k^{t-1}|k_p^t)}{\partial \phi_k^{t-1}}, \quad (12)$$

where the second term is the data-consistency update, the third term is the additional update based on the random kernel k_p^t .

It has been proved to be effective that the random noise-based disturbance can prevent being trapped into bad local modes for the variable update in Langevin dynamics [2, 32, 48, 51]. More details of Langevin dynamics refer to the supplementary material. At this stage, the random kernel sample from the RKS module can be regarded as the random “noise” for the ϕ_k^{t-1} update. Eq. (12) can be reformulated as follows,

$$\phi_k^t = \phi_k^{t-1} + \frac{\delta^2}{2} \frac{\partial \log p(\phi_k^{t-1}|\mathbf{x}^{t-1}, \mathbf{y})}{\partial \phi_k^{t-1}} + \zeta_{\phi_k}^{t-1}, \quad (13)$$

where $\zeta_{\phi_k}^{t-1} = \frac{\partial \log p(\phi_k^{t-1}|k_p^t)}{\partial \phi_k^{t-1}}$ denotes the parameters correlated Langevin dynamics disturbance.

The pipeline of our DKP at the t^{th} iteration is given in Algorithm 1. The whole DKP model is implemented in a plug-and-play style, in which training in advance is not required. Besides, the random kernels from the RKS module are self-adaptively sampled through the MCMC simulation, without the need of labeled training data. We should also note that the DKP model only brings neglectable runtime and memory cost in applications, as the adopted network G_k is typically lightweight. This leads to high flexibility and low computational complexity. These three merits promise our DKP the convenience of being applied to

Algorithm 1: The proposed DKP model.

- 1 **Given:** \mathbf{x}^{t-1} , \mathbf{y} and ϕ_k^{t-1} .
- 2 % Random Kernel Sampling (RKS) Module
- 3 Sample random kernels $\{k_r^l\}_{l=1}^L$ via MC.
- 4 **for** $l \leftarrow 0, 1, \dots, L$ **do**
- 5 $\omega^l = \frac{1}{\mathcal{L}_{MCMC}^l}$, $\mathcal{L}_{MCMC}^l = \|\mathbf{y} - (\mathbf{x}^{t-1} \otimes k_r^l)\|_{\downarrow s}^2 + \delta$
- 6 **end**
- 7 $k_p^t = \frac{1}{L} \sum_{l=1}^L \omega^l k_r^l$
- 8 % Prior Kernel Estimation (PKE) Module
- 9 $\phi_k^t = \phi_k^{t-1} + \frac{\delta^2}{2} \frac{\partial \log p(\phi_k^{t-1}|\mathbf{x}^{t-1}, \mathbf{y})}{\partial \phi_k^{t-1}} + \delta \frac{\partial \log p(\phi_k^{t-1}|k_p^t)}{\partial \phi_k^{t-1}}$
- 10 **Output:** $k^t = G_k(\phi_k^t)$.

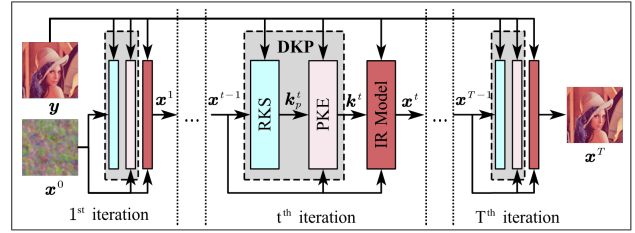


Figure 3. The overview of our DKP-based BSR method.

the existing image restoration approaches, including the untrained DIP model and off-the-shelf pre-trained diffusion model, which will be detailed in the next section.

4. DKP-based BSR Methods

4.1. Pipeline

The overview of the proposed DKP-based BSR method is illustrated in Fig. 3. The DKP model (gray box), including RKS module (blue box), PKE module (lilac box), and IR model (red box) alternatively optimize the blur kernel and refine the HR image, respectively. For each iteration, the estimated HR image x^{t-1} and LR image \mathbf{y} are first fed to RKS module f_{RKS} to generate kernel prior

$$k_p^t = f_{\text{RKS}}(\mathbf{x}^{t-1}, \mathbf{y}), \quad (14)$$

where x^{t-1} denotes the estimated HR image from the last IR model output. Then, the kernel prior k_p^t will be assigned to the PKE module f_{PKE} , which estimates kernel as follows,

$$k^t = f_{\text{PKE}}(\mathbf{x}^{t-1}, \mathbf{y}, k_p^t), \quad (15)$$

where k^t is the estimated kernel at the t^{th} kernel estimation iteration, which will be assigned to the IR model. The t^{th} HR image x^t can be estimated by the IR model as follows

$$x^t = f_{\text{IR}}(\mathbf{x}^{t-1}, \mathbf{y}, k^t), \quad (16)$$

where f_{IR} denotes the adopted IR model. In this paper, two representative IR models, DIP [44] and diffusion model [14], are applied to evaluate the DKP-based BSR solutions, referring to DIP-DKP and Diff-DKP, which are introduced in the sequel.

Algorithm 2: The proposed DIP-DKP.

```
1 Given:  $\mathbf{y}, \phi_x^0, \phi_{DKP}^0, \mathbf{x}^0 = G_x(\phi_x^0)$ .
2 for  $t \leftarrow 0, 1, \dots, T-1$  do
3   % DKP-based kernel estimation stage
4    $\phi_{DKP}^{t+1} = \phi_{DKP}^t + \frac{\delta^2}{2} \frac{\partial \log p(\phi_{DKP}^t | \mathbf{x}^t, \mathbf{y})}{\partial \phi_{DKP}^t} + \delta \frac{\partial \log p(\phi_{DKP}^t | \mathbf{k}_p^t)}{\partial \phi_{DKP}^t}$ 
5    $\mathbf{k}^{t+1} = G_{DKP}(\phi_{DKP}^{t+1})$ 
6   % DIP-based image restoration stage
7    $\phi_x^{t+1} = \phi_x^t + \gamma_x^t \frac{\partial \log p(\phi_x^t | \mathbf{y}, \mathbf{k}^t)}{\partial \phi_x^t}$ 
8    $\mathbf{x}^{t+1} = G_x(\phi_x^{t+1})$ 
9 end
10 Output:  $\mathbf{x}^T, \mathbf{k}^T$ .
```

4.2. The proposed DIP-DKP

DIP-based Image Restoration. DIP [44] is designed for capturing low-level image statistics, and estimates HR image $\mathbf{x} = G_x(\mathbf{z}_x, \phi_x)$ from a fixed random noise input \mathbf{z}_x (we omit \mathbf{z}_x in the rest of this paper for demonstration convenience). A typical formulation of DIP-based BSR methods [25, 34] is given as follows

$$\begin{cases} \phi_x^*, \phi_k^* = \arg \min_{\phi_x, \phi_k} \|\mathbf{y} - \\ \quad (G_x(\phi_x) \otimes G_k(\phi_k)) \downarrow_s\|_F^2, & (17) \\ \mathbf{x}^* = G_x(\phi_x^*), \mathbf{k}^* = G_k(\phi_k^*). & (18) \end{cases}$$

Double-DIP [34] and FKP-DIP [25] have exploited the effectiveness towards the BSR problem. However, the kernel prior of $G_k(\phi_k^*)$ either adopts the untrained network with limited performances on the kernel estimation [34], or pre-trained kernel network, referring to FKP [25], that requests supervised training in advance. As shall be shown in experiments, pre-trained networks do not perform well to generate reasonable kernel estimations when the kernel categories vary.

Proposed DIP-DKP. We replace the untrained or pre-trained networks for kernel priors in the existing DIP-based alternative framework by the proposed DKP model, which we refer to as DIP-DKP. The objective of our proposed DIP-DKP can be formulated as follows,

$$\begin{cases} \phi_x^*, \phi_{DKP}^* = \arg \min_{\phi_x, \phi_{DKP}} \|\mathbf{y} - (G_{DKP}(\phi_{DKP}) \otimes \\ \quad G_x(\phi_x)) \downarrow_s\|_F^2 + \|G_{DKP}(\phi_{DKP}) - \mathbf{k}_p\|_F^2, & (19) \\ \mathbf{x}^* = G_x(\phi_x^*), \mathbf{k}^* = G_{DKP}(\phi_{DKP}^*), & (20) \end{cases}$$

where $G_{DKP}(\phi_{DKP})$ is the kernel network of the proposed DKP model.

The overall solution procedure of the proposed DIP-DKP is given in Algorithm 2. At each t^{th} iteration, the kernel \mathbf{k}^t is estimated in the DKP-based kernel estimation stage and then is assigned to the DIP model for HR image

Algorithm 3: The proposed Diff-DKP.

```
1 Given:  $\mathbf{y}, \phi_{DKP}^T, S_\theta$  and  $\mathbf{x}_T \sim \mathcal{N}(\mathbf{0}, \mathbf{I})$ .
2 for  $t \leftarrow T, T-1, \dots, 1$  do
3   % Diffusion-based image restoration process
4    $\mathbf{x}_{0|t} = \frac{1}{\sqrt{\bar{\alpha}^t}}(\mathbf{x}_t - S_\theta(\mathbf{x}_t, t))\sqrt{1 - \bar{\alpha}^t}$ 
5   % DKP incorporated data consistency refinement
6    $\phi_{DKP}^{t-1} = \phi_{DKP}^t + \frac{\delta^2}{2} \frac{\partial \log p(\phi_{DKP}^t | \mathbf{x}_{0|t}, \mathbf{y})}{\partial \phi_{DKP}^t} + \delta \frac{\partial \log p(\phi_{DKP}^t | \mathbf{k}_p^t)}{\partial \phi_{DKP}^t}$ 
7    $\mathbf{k}^{t-1} = G_{DKP}(\phi_{DKP}^{t-1})$ 
8    $\hat{\mathbf{x}}_{0|t} = \mathbf{x}_{0|t} + \gamma_x^t \frac{\partial \log p(\mathbf{x}_{0|t} | \mathbf{y}, \mathbf{k}^{t-1})}{\partial \mathbf{x}_{0|t}}$ 
9    $\mathbf{x}_{t-1} \sim p(\mathbf{x}_{t-1} | \mathbf{x}_t, \hat{\mathbf{x}}_{0|t})$ 
10 end
11 Output:  $\mathbf{x}_0, \mathbf{k}^0$ .
```

restoration in the forward propagation. In the back propagation, the parameters of DIP and DKP, i.e., ϕ_x and ϕ_{DKP} , are updated while solving the BSR problem via an unsupervised inference. With DKP, DIP-DKP realizes an adaptive kernel learning along the convergence trajectory of the BSR objective function, enabling accurate and dynamic kernel estimation. Therefore, without expensive labeled data and long training time in advance, DIP-DKP can estimate HR image and blur kernel simultaneously in a plug-and-play style.

4.3. Diff-DKP

Original DDPM Inference Process. Denoising diffusion probabilistic models (DDPM) [14] defines a T-step forward process to add noise to data and a T-step reverse process to restore desired data from the noise. When an off-the-shelf DDPM S_θ is applied to solve image restoration problem, the reverse process is implemented as inference process to estimate the high quality image as follows,

$$\begin{cases} \mathbf{x}_{0|t} = \frac{1}{\sqrt{\bar{\alpha}^t}}(\mathbf{x}_t - S_\theta(\mathbf{x}_t, t))\sqrt{1 - \bar{\alpha}^t}, & (21) \\ \mathbf{x}_{t-1} \sim p(\mathbf{x}_{t-1} | \mathbf{x}_t, \mathbf{x}_{0|t}), & (22) \end{cases}$$

where $\mathbf{x}_{0|t}$ denotes the estimated HR image \mathbf{x}_0 at the t^{th} step, and $\bar{\alpha}^t$ is the hyper-parameter. To ensure that HR images $\mathbf{x}_0 \sim q(\mathbf{x})$ can be reconstructed from random noise $\mathbf{x}_T \sim \mathcal{N}(\mathbf{0}, \mathbf{I})$, the existing methods typically re-train [38] or fine-tune [50] the DDPM model via supervised learning on LR-HR datasets, or provide ground truth kernel [46] to enroll task-specific knowledge for convergence guarantee. However, the performance of DDPM is unstable, even when trained by a large number of labeled dataset.

Proposed Diff-DKP. The instability of DDPM mainly comes from the training process that involves multiple image processing tasks. In this case, the off-the-shelf diffusion model cannot concentrate on BSR objective, thus leading to

image distortion and content mismatch. To alleviate this issue, the proposed Diff-DKP incorporates the DKP model to provide task-specific data-consistency knowledge on the basis of the vanilla DDPM reverse iterations. Specifically, an external DKP incorporated data consistency refinement of $\mathbf{x}_{0|t}$ is inserted between (21) and (22), given by

$$\hat{\mathbf{x}}_{0|t} = \mathbf{x}_{0|t} + \gamma_{\mathbf{x}}^t \frac{\partial \log p(\mathbf{x}_{0|t} | \mathbf{y}, \mathbf{k}^t)}{\partial \mathbf{x}_{0|t}}, \quad (23)$$

where $\gamma_{\mathbf{x}}^t$ is the update step, and

$$\log p(\mathbf{x}_{0|t} | \mathbf{y}, \mathbf{k}^t) = -\|\mathbf{y} - (\mathbf{x}_{0|t} \otimes \mathbf{k}^t) \downarrow_s\|_F^2, \quad (24)$$

which enables the inference process to converge to the right direction along with the data-consistent solution.

The overview of the Diff-DKP algorithm is presented in Algorithm 3. Let $t = T, T - 1, \dots, 1$ denote the index of the diffusion reverse step. At each step, the diffusion model first estimates the $\mathbf{x}_{0|t}$. Then, the DKP model adaptively generates kernel prior with respect to the latest $\mathbf{x}_{0|t}$, while $\mathbf{x}_{0|t}$ is further updated with respect to the data consistency Eq. (24), thus, ensuring the inference process is underlying the BSR objective. It is noteworthy to point out that the parameters of the diffusion model are fixed and only the parameters of lightweight kernel estimator network are optimized in the inference process.

In this way, the off-the-shelf diffusion model plays the role of HR image estimator, while the estimated HR image is further refined by the BSR task specific prior knowledge, referring to Eq. (23). Different from those methods that incorporate prior knowledge of BSR task via supervised re-training/fine-tuning, Diff-DKP behaves a plug-and-play scheme, thus without data demands and training cost before implementation.

5. Experiments

5.1. Experimental Setup

Data Preparation. Following the widely adopted kernel assumption [25, 35, 45, 51], we conduct the experiments on anisotropic Gaussian kernels and motion kernels, which are shown in Fig. 4. The kernel sizes are set to $(4s + 3) \times (4s + 3)$. For the Gaussian kernel, the width ranges are set to $[0.175s, 2.5s]$, and the rotation angle range is set to $[0, \pi]$, with a scale factor $s = 4$, respectively. For the motion kernel, we adopt random motion kernel generation method proposed by [22], which simulates realistic and complex blur kernels from random trajectories. Detailed formulations of Gaussian and motion kernels are given in the supplementary material. We synthesize LR images with random kernels with respect to Eq. (1) for testing data based on five popular public benchmark datasets, including Set5 [4], Set14 [52], BSD100 [30], Urban100 [15] and RealSRSet [23]. We compare these kernels in terms of the peak

signal to noise ratio (PSNR), and compare HR images in terms of PSNR and structural similarity (SSIM) [47].

Comparison Methods. The proposed DIP-DKP and Diff-DKP are compared with existing baselines including: Double-DIP [34], DIP-FKP [25], DASR [45], BSRDM [51], DCLS [29], DARM [58] and DiffBSR [26]. Specifically, Double-DIP tends to provide kernel priors by training a FCN network only with respect to the LR image restoration error. DIP-FKP incorporates the FKP model as kernel prior which is pre-trained on kernel datasets. KernelGAN+ZSSR and DARM are self-supervised and train an interal generative adversarial network (GAN) to estimate the blur kernel. BSRDM formulates an elaborate degradation modelling on noise and kernel as handcrafted priors. DASR is a representative end-to-end method that is pre-trained on DIV2K [1] and Flickr2K [43] HR image datasets. DiffBSR is fine-tuned on BSR labeled datasets before applied to estimate HR images.

Implementation and Hyper-parameters. The adopted kernel estimation network G_k of PKE module in this paper is a three-layer fully-connected network (FCN). The adopted DIP model follows the original settings in [44], and the diffusion model is the vanilla version [14] that is trained on ImageNet [6]. The number of sampling times in the MCMC simulation L is the only hyper-parameter in the proposed DKP model. The hyper-parameter tuning results are given in Table 1. It is explicit that the performance reaches equilibrium around $L \in [4, 8]$. To balance the efficiency and effectiveness, we set $L = 5$ in this paper.

5.2. Comparison with State-of-the-Arts

Evaluation on Gaussian Kernel Scenario. Quantitative evaluation results on four datasets with scale factors $s = 4$ are presented in the upper half part of Table 2. We can see that the proposed DIP-DKP and Diff-DKP achieve the second and the best results on all datasets. We note that DIP-DKP only realizes slightly higher performance than the existing state-of-the-art (SotA) methods, while Diff-DKP achieves significantly better performances. This recalls our demonstrations in Section 4: DIP-DKP is totally trained while solving from scratch, and the DKP model plays the role of providing better convergence guarantee. Diff-DKP utilizes the DKP model to guide the well-trained diffusion model with fruitful data priors to converge to BSR task for better HR image restoration performances. In Table 3, we further show that our DKP model achieves the accurate ker-

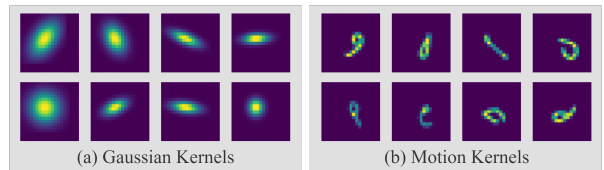


Figure 4. The visualization of the adopted blur kernels.

Table 1. Average image PSNR performance of the proposed DIP-DKP and Diff-DKP on Set5 [4] on the Gaussian kernel scenario.

Methods	$L = 0$	$L = 2$	$L = 4$	$L = 6$	$L = 8$	$L = 10$	$L = 15$
DIP-DKP (Ours)	20.99	27.12	28.44	28.57	28.52	28.29	28.03
Diff-DKP (Ours)	21.97	28.95	29.40	29.47	29.76	29.67	29.26

Table 2. Average PSNR/SSIM of different methods on public datasets that are synthesized by the random Gaussian/Motion kernels with $s = 4$. The best and second best results are highlighted in red and blue colors, respectively.

Method	Kernel	Set5 [4]	Set14 [52]	BSD100 [30]	Urban100 [15]
Double-DIP [34]	Gaussian kernel scenario	20.99/0.5578	18.31/0.4426	18.57/0.3815	18.15/0.4491
DASR [45]		27.37/0.7859	25.43/0.6591	25.11/0.6129	22.88/0.6448
DIP-FKP [25]		27.77/0.7914	25.65/0.6764	25.15/0.6354	22.89/0.6327
BSRDM [51]		27.81/0.8029	25.35/0.6859	25.61/0.6526	22.36/0.6601
DCLS [29]		27.50/0.7948	25.68/0.6639	25.34/0.6169	22.92/0.6475
DiffBIR [26]		25.15/0.6468	23.01/0.5935	23.88/0.5586	21.94/0.5657
DARM [58]		26.25/0.6818	24.19/0.6187	24.29/0.5898	22.14/0.5967
DIP-DKP (Ours)		28.03/0.8039	25.98/0.6878	25.66/0.6531	23.24/0.6644
Diff-DKP (Ours)		29.44/0.8592	26.76/0.7400	26.63/0.7057	23.92/0.6875
Double-DIP [34]		Motion kernel scenario	18.92/0.4510	20.41/0.4847	19.00/0.3757
DASR [45]	24.21/0.7252		24.16/0.6145	22.47/0.5836	20.24/0.5478
DIP-FKP [25]	24.61/0.7371		24.21/0.6227	22.80/0.5880	20.33/0.5572
BSRDM [51]	24.01/0.7098		23.56/0.6009	22.62/0.5791	20.40/0.5494
DCLS [29]	24.78/0.7323		24.38/0.6211	22.74/0.5922	20.49/0.5534
DiffBIR [26]	23.63/0.6367		23.59/0.6043	22.35/0.5784	20.14/0.5347
DARM [58]	24.23/0.7269		23.95/0.6294	22.48/0.5830	20.58/0.5595
DIP-DKP (Ours)	25.30/0.7417		24.52/0.6434	23.02/0.6136	21.24/0.5667
Diff-DKP (Ours)	28.74/0.8313		26.03/0.6719	24.10/0.6287	22.26/0.5862

nel estimation with higher kernel PSNR.

Evaluation on Motion Kernel Scenario. The lower half part of Table 2 shows the simulation results on the motion kernel scenario. The supervised learning methods, i.e., DASR and DiffBIR, are re-trained/fine-tuned on motion kernel degraded HR image datasets. DIP-FKP is re-trained on the motion kernel dataset. The proposed DIP-DKP and Diff-DKP show significantly better performance on the motion kernel scenario, which validates that the proposed DKP model has good generalization ability towards different kernel categories. Specifically, Diff-DKP presents stable PSNR/SSIM scores when being applied to estimate motion kernels, while the rest suffer significant performance drop. This indicates that the proposed DKP is expected to handle kernel varying tasks.

Visual Results. The visual results of different methods on synthetic and real-world images are shown in Fig. 5. We can see that 1) In the case of Gaussian kernel, all methods are capable of producing satisfactory deblurring results, while our DIP-DKP and Diff-DKP yield better results with more accurate kernel estimation. 2) In the case of motion kernel, certain distortion on the estimated kernel can be seen in FKP-DKP and BSRDM fail to estimate motion kernel. Meanwhile, our DIP-DKP and Diff-DKP achieve approximately accurate motion kernel estimation. 3) In the case of real image, both DIP-FKP and BSRDM estimate the Gaussian-like kernels, whereas our DIP-DKP and Diff-DKP tend to estimate the non-Gaussian kernels. This verifies that an adaptive and flexible kernel estimation discipline is learned by our DKP model, which may fit the real-world applications better.

Table 3. Average PSNR/SSIM of images and PSNR of kernels on Set14 [52] with $s = 4$. The best and second best results are highlighted in red and blue colors, respectively.

Method	Kernel	Kernel PSNR	Image PSNR/SSIM	
DIP-DKP without RKS	Gaussian kernel scenario	37.92	18.77/0.4227	
Diff-DKP without RKS		40.93	17.33/0.3408	
Double-DIP [34]		50.62	18.31/0.4426	
DIP-FKP [25]		54.46	25.65/0.6764	
BSRDM [51]		55.38	25.35/0.6859	
DIP-DKP (Ours)		56.20	25.98/0.6878	
Diff-DKP (Ours)		56.76	26.76/0.7400	
DIP-DKP without RKS		Motion kernel scenario	34.92	18.19/0.4223
Diff-DKP without RKS			34.78	17.65/0.3513
Double-DIP [34]			35.52	20.41/0.4847
DIP-FKP [25]	37.52		24.21/0.6227	
BSRDM [51]	37.88		23.56/0.6009	
DIP-DKP (Ours)	39.33		24.52/0.6434	
Diff-DKP (Ours)	40.37	26.03/0.6719		

5.3. Ablation Studies

Ablation study of RKS module. The ablation studies are carried on the MCMC sampling of kernel priors. “Without RKS” denotes that the adopted DKP updates the kernel network only by the data-consistency term without the learned kernel prior. In Fig. 6 (left), it can be seen that the estimated kernels without RKS have significant distortion, leading to remarkable PSNR drop of the estimated HR image, while DIP-DKP can estimate Gaussian kernels precisely with respect to the ground truth (with red frame). Fig. 6 (right) shows that the accurate motion kernel estimation no longer exists when the RKS module is absent. It is thus obvious that without the kernel prior learned from the MCMC process, the Diff-DKP fails to converge to a rational motion kernel estimation. The average kernel and image results are shown in Table 3. Without kernel prior learned from the RKS module, the kernel estimation performances of DKP-

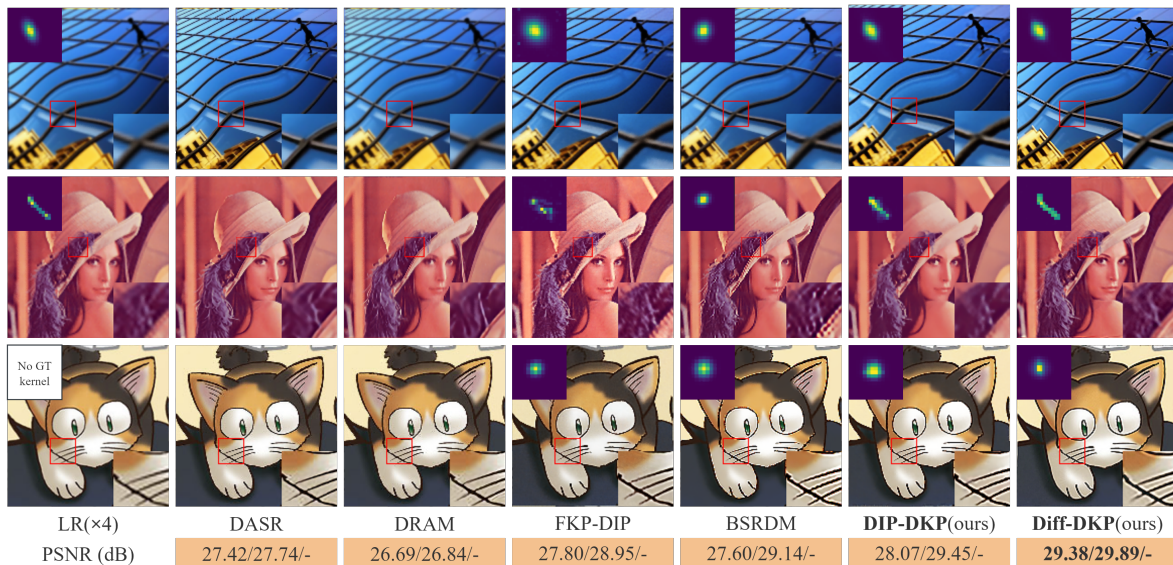


Figure 5. Visual results of different methods on public datasets for scale factor 4. Estimated/ground-truth kernels are shown on the top left.

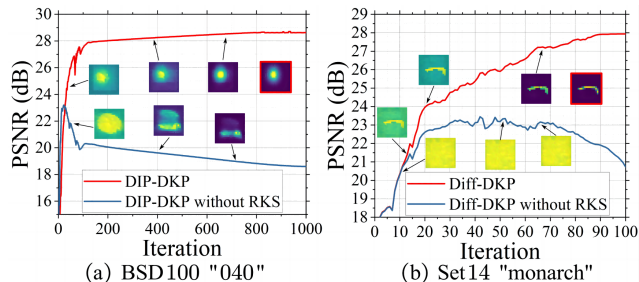


Figure 6. The intermediate results of DIP-DKP, Diff-DKP and their no RKS module versions over iterations on two test images.

Table 4. The ablation of PKE module. (Set5, x4, image PSNR)

Layers\Units	10	100	1000	10000
1	13.75	23.57	28.93	28.24
3	13.61	28.97	28.48	28.35
5	13.30	28.81	28.52	26.65
7	13.86	28.30	28.54	27.93

based BSR methods have a significant performance drop, leading to poor image restoration performance as well.

Ablation study of PKE module. Since PKE essentially estimates blur kernels on the basis of the random kernel priors and LR observations, thus it is indispensable and we conduct ablation study on the different structures of kernel network in PKE module in Table 4. We find that the kernel network performs well when it has 3-7 layers with 100-1000 units in each layer. This indicates that the kernel network has good generalization-ability for the structure without the necessity of elaborately designing the network.

5.4. Model Size, Runtime and Memory Usage

The kernel network of our DKP model has a total of 562K parameters (FLOPs: 536K) while Double-DIP and DIP-FKP have 641K parameters (FLOPs: 600K) and 143K parameters (FLOPs: 178K), respectively. The runtime and memory usage of our DIP-DKP on a GeForce RTX 3090

GPU for generating a HR image of size 512×512 are about 92 seconds and 11GB memory, which is comparable with the Double-DIP (91 seconds and 11.2GB) and DIP-FKP (90 seconds and 10.6GB). As for Diff-DKP, the 512×512 image needs to be divided into four 256×256 images for restoration, which costs a total of 60 seconds and 4GB memory. Considering that our DIP-DKP and Diff-DKP are unsupervised and plug-and-play, it is reasonable to say that our methods have moderate computational costs.

Due to the page limitations, more experimental results are given in the supplementary material.

6. Conclusion

In this paper, we propose a dynamic kernel prior (DKP) model to solve the BSR problem in an unsupervised and pre-training-free paradigm. DKP realizes the rational kernel prior learning from MCMC sampling on random kernel distributions, providing accurate kernel estimation and thus leading to better HR image restoration. DKP can be easily incorporated with existing image restoration model, such as DIP and diffusion model, by replacing their kernel modeling modules or adding as an external kernel prior generator. When applied to solve the BSR problem, DKP is trained while solving the task with respect to the LR image restoration error, enabling no training necessity and labeled data demands. Extensive experiments on Gaussian and motion kernel scenarios with synthetic LR images and real-world images validate that DKP-based methods improve the kernel estimation accuracy significantly and thus lead to superior BSR results. We believe that the concept of using a trainable sampling process to provide adaptive priors will lead to a new direction in solving low-level tasks, aiming to achieve superior performance with modest computational costs in the way of unsupervised inference.

References

- [1] Eirikur Agustsson and Radu Timofte. Ntire 2017 challenge on single image super-resolution: Dataset and study. In *Proceedings of the IEEE conference on computer vision and pattern recognition workshops*, pages 126–135, 2017. 6
- [2] Dominique Bakry and Michel Émery. Diffusions hypercontractives. In *Séminaire de Probabilités XIX 1983/84: Proceedings*, pages 177–206. Springer, 2006. 4
- [3] Sefi Bell-Kligler, Assaf Shocher, and Michal Irani. Blind super-resolution kernel estimation using an internal-gan. *Advances in Neural Information Processing Systems*, 32, 2019. 1, 2
- [4] Marco Bevilacqua, Aline Roumy, Christine Guillemot, and Marie Line Alberi-Morel. Low-complexity single-image super-resolution based on nonnegative neighbor embedding. In *British Machine Vision Conference*, pages 135–1, 2012. 6, 7
- [5] Hyungjin Chung, Jeongsol Kim, Michael T Mccann, Marc L Klasky, and Jong Chul Ye. Diffusion posterior sampling for general noisy inverse problems. *arXiv preprint arXiv:2209.14687*, 2022. 1, 2
- [6] Jia Deng, Wei Dong, Richard Socher, Li-Jia Li, Kai Li, and Li Fei-Fei. Imagenet: A large-scale hierarchical image database. In *2009 IEEE conference on computer vision and pattern recognition*, pages 248–255. Ieee, 2009. 6
- [7] Chao Dong, Chen Change Loy, Kaiming He, and Xiaoou Tang. Learning a deep convolutional network for image super-resolution. In *European conference on computer vision*, pages 184–199. Springer, 2014. 2
- [8] Yangyi Dong, Xiaoyun Zhang, Zhixin Wang, Ya Zhang, Siheng Chen, and Yanfeng Wang. Unpaired face restoration via learnable cross-quality shift. In *Proceedings of the IEEE/CVF Conference on Computer Vision and Pattern Recognition*, pages 667–675, 2022. 3
- [9] Netalee Efrat, Daniel Glasner, Alexander Apartsin, Boaz Nadler, and Anat Levin. Accurate blur models vs. image priors in single image super-resolution. In *Proceedings of the IEEE International Conference on Computer Vision*, pages 2832–2839, 2013. 3
- [10] Yosef Gandelsman, Assaf Shocher, and Michal Irani. ”double-dip”: Unsupervised image decomposition via coupled deep-image-priors. In *Proceedings of the IEEE/CVF Conference on Computer Vision and Pattern Recognition*, pages 11026–11035, 2019. 2
- [11] Daniel Glasner, Shai Bagon, and Michal Irani. Super-resolution from a single image. In *2009 IEEE 12th international conference on computer vision*, pages 349–356. IEEE, 2009. 2
- [12] Jinjin Gu, Hannan Lu, Wangmeng Zuo, and Chao Dong. Blind super-resolution with iterative kernel correction. In *Proceedings of the IEEE/CVF Conference on Computer Vision and Pattern Recognition*, pages 1604–1613, 2019. 1, 2, 3
- [13] Lanqing Guo, Chong Wang, Wenhan Yang, Siyu Huang, Yufei Wang, Hanspeter Pfister, and Bihan Wen. Shadowdiffusion: When degradation prior meets diffusion model for shadow removal. In *Proceedings of the IEEE/CVF Conference on Computer Vision and Pattern Recognition*, pages 14049–14058, 2023. 1
- [14] Jonathan Ho, Ajay Jain, and Pieter Abbeel. Denoising diffusion probabilistic models. *Advances in neural information processing systems*, 33:6840–6851, 2020. 2, 3, 4, 5, 6
- [15] Jia-Bin Huang, Abhishek Singh, and Narendra Ahuja. Single image super-resolution from transformed self-exemplars. In *Proceedings of the IEEE conference on computer vision and pattern recognition*, pages 5197–5206, 2015. 6, 7
- [16] Yan Huang, Shang Li, Liang Wang, Tieniu Tan, et al. Unfolding the alternating optimization for blind super resolution. *Advances in Neural Information Processing Systems*, 33:5632–5643, 2020. 1, 2
- [17] Meiguang Jin, Stefan Roth, and Paolo Favaro. Normalized blind deconvolution. In *Proceedings of the European Conference on Computer Vision (ECCV)*, pages 668–684, 2018. 1
- [18] Jiwon Kim, Jung Kwon Lee, and Kyoung Mu Lee. Accurate image super-resolution using very deep convolutional networks. In *Proceedings of the IEEE conference on computer vision and pattern recognition*, pages 1646–1654, 2016. 2
- [19] Kwang In Kim and Younghee Kwon. Single-image super-resolution using sparse regression and natural image prior. *IEEE transactions on pattern analysis and machine intelligence*, 32(6):1127–1133, 2010. 1, 2
- [20] Soo Ye Kim, Hyeonjun Sim, and Munchurl Kim. Koalantet: Blind super-resolution using kernel-oriented adaptive local adjustment. In *Proceedings of the IEEE/CVF conference on computer vision and pattern recognition*, pages 10611–10620, 2021. 1, 2
- [21] Dilip Krishnan and Rob Fergus. Fast image deconvolution using hyper-laplacian priors. *Advances in neural information processing systems*, 22, 2009. 1, 2
- [22] Orest Kupyn, Volodymyr Budzan, Mykola Mykhailych, Dmytro Mishkin, and Jiří Matas. Deblurgan: Blind motion deblurring using conditional adversarial networks. In *Proceedings of the IEEE conference on computer vision and pattern recognition*, pages 8183–8192, 2018. 6
- [23] Yuelong Li, Mohammad Tofiqi, Junyi Geng, Vishal Monga, and Yonina C Eldar. Efficient and interpretable deep blind image deblurring via algorithm unrolling. *IEEE Transactions on Computational Imaging*, 6:666–681, 2020. 6
- [24] Yawei Li, Yuchen Fan, Xiaoyu Xiang, Denis Demandolx, Rakesh Ranjan, Radu Timofte, and Luc Van Gool. Efficient and explicit modelling of image hierarchies for image restoration. In *Proceedings of the IEEE/CVF Conference on Computer Vision and Pattern Recognition*, pages 18278–18289, 2023. 2
- [25] Jingyun Liang, Kai Zhang, Shuhang Gu, Luc Van Gool, and Radu Timofte. Flow-based kernel prior with application to blind super-resolution. In *Proceedings of the IEEE/CVF Conference on Computer Vision and Pattern Recognition*, pages 10601–10610, 2021. 1, 2, 3, 5, 6, 7
- [26] Xinqi Lin, Jingwen He, Ziyang Chen, Zhaoyang Lyu, Ben Fei, Bo Dai, Wanli Ouyang, Yu Qiao, and Chao Dong. Diffbir: Towards blind image restoration with generative diffusion prior. *arXiv preprint arXiv:2308.15070*, 2023. 2, 6, 7

- [27] Jie Liu, Wenjie Zhang, Yuting Tang, Jie Tang, and Gangshan Wu. Residual feature aggregation network for image super-resolution. In *Proceedings of the IEEE/CVF conference on computer vision and pattern recognition*, pages 2359–2368, 2020. 1
- [28] Zhengxiong Luo, Yan Huang, Shang Li, Liang Wang, and Tieniu Tan. End-to-end alternating optimization for blind super resolution. *arXiv preprint arXiv:2105.06878*, 2021. 2
- [29] Ziwei Luo, Haibin Huang, Lei Yu, Youwei Li, Haoqiang Fan, and Shuaicheng Liu. Deep constrained least squares for blind image super-resolution. In *Proceedings of the IEEE/CVF Conference on Computer Vision and Pattern Recognition*, pages 17642–17652, 2022. 1, 2, 6, 7
- [30] David Martin, Charless Fowlkes, Doron Tal, and Jitendra Malik. A database of human segmented natural images and its application to evaluating segmentation algorithms and measuring ecological statistics. In *Proceedings Eighth IEEE International Conference on Computer Vision. ICCV 2001*, pages 416–423. IEEE, 2001. 6, 7
- [31] Tomer Michaeli and Michal Irani. Nonparametric blind super-resolution. In *Proceedings of the IEEE International Conference on Computer Vision*, pages 945–952, 2013. 2
- [32] Radford M Neal et al. Mcmc using hamiltonian dynamics. *Handbook of markov chain monte carlo*, 2(11):2, 2011. 4
- [33] Daniele Perrone and Paolo Favaro. A clearer picture of total variation blind deconvolution. *IEEE transactions on pattern analysis and machine intelligence*, 38(6):1041–1055, 2015. 1, 2
- [34] Dongwei Ren, Kai Zhang, Qilong Wang, Qinghua Hu, and Wangmeng Zuo. Neural blind deconvolution using deep priors. In *Proceedings of the IEEE/CVF Conference on Computer Vision and Pattern Recognition*, pages 3341–3350, 2020. 1, 2, 5, 6, 7
- [35] Gernot Riegler, Samuel Schulter, Matthias Ruther, and Horst Bischof. Conditioned regression models for non-blind single image super-resolution. In *Proceedings of the IEEE International Conference on Computer Vision*, pages 522–530, 2015. 6
- [36] Leonid I Rudin, Stanley Osher, and Emad Fatemi. Nonlinear total variation based noise removal algorithms. *Physica D: nonlinear phenomena*, 60(1-4):259–268, 1992. 2
- [37] Marshall F Tappen Bryan C Russell and William T Freeman. Exploiting the sparse derivative prior for super-resolution and image demosaicing. In *Proceedings of the Third International Workshop Statistical and Computational Theories of Vision*, pages 1–28, 2003. 2
- [38] Chitwan Saharia, Jonathan Ho, William Chan, Tim Salimans, David J Fleet, and Mohammad Norouzi. Image super-resolution via iterative refinement. *IEEE Transactions on Pattern Analysis and Machine Intelligence*, 45(4):4713–4726, 2022. 2, 5
- [39] Assaf Shocher, Nadav Cohen, and Michal Irani. “zero-shot” super-resolution using deep internal learning. In *Proceedings of the IEEE conference on computer vision and pattern recognition*, pages 3118–3126, 2018. 1, 2
- [40] Jiaming Song, Arash Vahdat, Morteza Mardani, and Jan Kautz. Pseudoinverse-guided diffusion models for inverse problems. In *International Conference on Learning Representations*, 2022. 1, 2
- [41] Yang Song and Stefano Ermon. Generative modeling by estimating gradients of the data distribution. *Advances in neural information processing systems*, 32, 2019. 3
- [42] Jian Sun, Zongben Xu, and Heung-Yeung Shum. Image super-resolution using gradient profile prior. In *2008 IEEE Conference on Computer Vision and Pattern Recognition*, pages 1–8. IEEE, 2008. 2
- [43] Radu Timofte, Eirikur Agustsson, Luc Van Gool, Ming-Hsuan Yang, and Lei Zhang. Ntire 2017 challenge on single image super-resolution: Methods and results. In *Proceedings of the IEEE conference on computer vision and pattern recognition workshops*, pages 114–125, 2017. 6
- [44] Dmitry Ulyanov, Andrea Vedaldi, and Victor Lempitsky. Deep image prior. In *Proceedings of the IEEE conference on computer vision and pattern recognition*, pages 9446–9454, 2018. 2, 3, 4, 5, 6
- [45] Longguang Wang, Yingqian Wang, Xiaoyu Dong, Qingyu Xu, Jungang Yang, Wei An, and Yulan Guo. Unsupervised degradation representation learning for blind super-resolution. In *Proceedings of the IEEE/CVF Conference on Computer Vision and Pattern Recognition*, pages 10581–10590, 2021. 2, 6, 7
- [46] Yinhuai Wang, Jiwen Yu, and Jian Zhang. Zero-shot image restoration using denoising diffusion null-space model. *arXiv preprint arXiv:2212.00490*, 2022. 2, 5
- [47] Zhou Wang, Alan C Bovik, Hamid R Sheikh, and Eero P Simoncelli. Image quality assessment: from error visibility to structural similarity. *IEEE transactions on image processing*, 13(4):600–612, 2004. 6
- [48] Max Welling and Yee W Teh. Bayesian learning via stochastic gradient langevin dynamics. In *Proceedings of the 28th international conference on machine learning (ICML-11)*, pages 681–688, 2011. 4
- [49] Yu-Syuan Xu, Shou-Yao Roy Tseng, Yu Tseng, Hsien-Kai Kuo, and Yi-Min Tsai. Unified dynamic convolutional network for super-resolution with variational degradations. In *Proceedings of the IEEE/CVF Conference on Computer Vision and Pattern Recognition*, pages 12496–12505, 2020. 1, 2
- [50] Xunpeng Yi, Han Xu, Hao Zhang, Linfeng Tang, and Jiayi Ma. Diff-retinex: Rethinking low-light image enhancement with a generative diffusion model. In *Proceedings of the IEEE/CVF International Conference on Computer Vision*, pages 12302–12311, 2023. 1, 2, 5
- [51] Zongsheng Yue, Qian Zhao, Jianwen Xie, Lei Zhang, Deyu Meng, and Kwan-Yee K. Wong. Blind image super-resolution with elaborate degradation modeling on noise and kernel. In *Proceedings of the IEEE/CVF Conference on Computer Vision and Pattern Recognition*, pages 2128–2138, 2022. 1, 2, 3, 4, 6, 7
- [52] Roman Zeyde, Michael Elad, and Matan Protter. On single image scale-up using sparse-representations. In *International conference on curves and surfaces*, pages 711–730. Springer, 2010. 6, 7

- [53] Kai Zhang, Wangmeng Zuo, and Lei Zhang. Learning a single convolutional super-resolution network for multiple degradations. In *Proceedings of the IEEE Conference on Computer Vision and Pattern Recognition*, pages 3262–3271, 2018. [1](#), [2](#), [3](#)
- [54] Kai Zhang, Luc Van Gool, and Radu Timofte. Deep unfolding network for image super-resolution. In *Proceedings of the IEEE/CVF conference on computer vision and pattern recognition*, pages 3217–3226, 2020. [1](#)
- [55] Kai Zhang, Yawei Li, Wangmeng Zuo, Lei Zhang, Luc Van Gool, and Radu Timofte. Plug-and-play image restoration with deep denoiser prior. *IEEE Transactions on Pattern Analysis and Machine Intelligence*, 44(10):6360–6376, 2021. [3](#)
- [56] Yulun Zhang, Kungpeng Li, Kai Li, Lichen Wang, Bineng Zhong, and Yun Fu. Image super-resolution using very deep residual channel attention networks. In *Proceedings of the European conference on computer vision (ECCV)*, pages 286–301, 2018. [1](#), [2](#)
- [57] Zixiang Zhao, Haowen Bai, Yuanzhi Zhu, Jianshe Zhang, Shuang Xu, Yulun Zhang, Kai Zhang, Deyu Meng, Radu Timofte, and Luc Van Gool. Ddfm: denoising diffusion model for multi-modality image fusion. *arXiv preprint arXiv:2303.06840*, 2023. [1](#), [2](#)
- [58] Hongyang Zhou, Xiaobin Zhu, Jianqing Zhu, Zheng Han, Shi-Xue Zhang, Jingyan Qin, and Xu-Cheng Yin. Learning correction filter via degradation-adaptive regression for blind single image super-resolution. In *Proceedings of the IEEE/CVF International Conference on Computer Vision*, pages 12365–12375, 2023. [2](#), [6](#), [7](#)
- [59] Yuanzhi Zhu, Kai Zhang, Jingyun Liang, Jiezhong Cao, Bihan Wen, Radu Timofte, and Luc Van Gool. Denoising diffusion models for plug-and-play image restoration. In *Proceedings of the IEEE/CVF Conference on Computer Vision and Pattern Recognition*, pages 1219–1229, 2023. [1](#), [2](#)